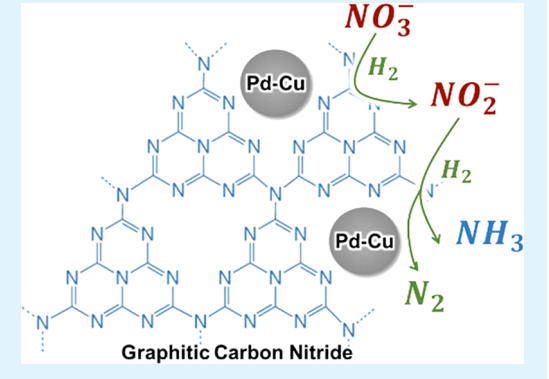


Graphitic Carbon Nitride Supported Ultrafine Pd and Pd—Cu Catalysts: Enhanced Reactivity, Selectivity, and Longevity for Nitrite and Nitrate Hydrogenation

Tao Ye, [†] David P. Durkin, [‡] Nathan A. Banek, [§] Michael J. Wagner, [§] and Danmeng Shuai*, [†]

Supporting Information

ABSTRACT: Novel Pd-based catalysts (i.e., Pd and Pd–Cu) supported on graphitic carbon nitride (g- C_3N_4) were prepared for nitrite and nitrate hydrogenation. The catalysts prepared by ethylene glycol reduction exhibited ultrafine Pd and Pd–Cu nanoparticles (~2 nm), and they showed high reactivity, high selectivity toward nitrogen gas over byproduct ammonium, and excellent stability over multiple reaction cycles. The unique nitrogenabundant surface, porous structure, and hydrophilic nature of g- C_3N_4 facilitates metal nanoparticle dispersion, mass transfer of reactants, and nitrogen coupling for nitrogen gas production to improve catalytic performance.



KEYWORDS: graphitic carbon nitride, Pd, Pd-Cu, nitrite, nitrate, catalytic hydrogenation, water treatment

Graphitic carbon nitride (g- C_3N_4) has emerged as a promising photocatalyst for selective oxidation, water splitting, environmental remediation, and renewable fuel production. Beyond the scope of photocatalysis, g- C_3N_4 has several unique properties to serve as an excellent catalyst support for metals. First, g- C_3N_4 is hydrophilic and has abundant N-containing functional groups (e.g., $-NH_2$, triazine) as basic coordination sites that facilitate metal nanoparticle (NP) dispersion. Second, the surface area and pore size of g- C_3N_4 can be tailored to promote uniform NP loading. Third, g- C_3N_4 can be synthesized from earth abundant precursors (e.g., urea, melamine), the synthesis process is facile and scalable, and the material is stable and environmentally benign. 1,2

Herein, we synthesized and characterized g-C₃N₄ supported monometallic Pd and bimetallic Pd-Cu NPs, with varied metal compositions, support properties, and metal loading methods, and evaluated their catalytic activity, selectivity, and longevity for nitrite and nitrate hydrogenation. Few studies of g-C₃N₄ supported metal catalysts for contaminant hydrogenation have been reported to date, ³⁻⁵ and this is the first report of bimetal NPs supported on g-C₃N₄ developed for contaminant removal and the systematic evaluation of their catalytic performance. Nitrite and nitrate contamination resulted from the intensive use of fertilizers, inappropriate disposal of animal wastes and septic tank effluents, and the discharge of industrial effluents, and the U.S. Environmental Protection Agency has regulated the contaminant concentration in drinking water to prevent

adverse human health impacts after digestion.⁶ Pd-based catalytic hydrogenation has emerged as a promising technology for the removal of nitrite and nitrate in drinking water and ion exchange brines for environmental remediation.^{7–9} A promoter metal (e.g., Cu, Sn, or In), in direct contact or in close proximity with Pd, is required to enable nitrate reduction to nitrite, while further reduction of nitrite to nitrogen gas or byproduct ammonia/ammonium only needs Pd (Scheme 1).⁷

Scheme 1. Nitrate Reduction Pathway on Pd-Based Catalysts a

$$NO_{3} \xrightarrow{Pd/Cu,In,Sn} NO_{2} \xrightarrow{Pd} \overbrace{H_{2}}^{Pd} NO_{2} \xrightarrow{Pd} \underbrace{NO_{1}}^{Pd} \underbrace{Pd}_{H_{2}} NO_{2}$$

$$NO_{3} \xrightarrow{Pd/Cu,In,Sn} NO_{2} \xrightarrow{Pd} \underbrace{NO_{1}}_{H_{2}} \underbrace{Pd}_{H_{2}} NO_{2}$$

$$NO_{3} \xrightarrow{Pd/Cu,In,Sn} NO_{2} \xrightarrow{Pd} \underbrace{NO_{1}}_{H_{2}} \underbrace{Pd}_{H_{2}} NO_{2}$$

$$NO_{3} \xrightarrow{Pd/Cu,In,Sn} NO_{2} \xrightarrow{Pd} \underbrace{NO_{1}}_{H_{2}} \underbrace{NO_{1}} \underbrace{NO_{1}}_{H_{2}} \underbrace{NO_{1}}_{H_{2}} \underbrace{NO_{1}}_{H_{2}} \underbrace{N$$

"NO is a proposed intermediate. Adapted with permission from ref 10. Copyright 2013 ChemCatChem.

Received: June 26, 2017 Accepted: August 10, 2017 Published: August 10, 2017

[†]Department of Civil and Environmental Engineering, The George Washington University, Washington, D.C. 20052, United States

[‡]Department of Chemistry, Johns Hopkins University, Baltimore, Maryland 21218, United States

[§]Department of Chemistry, The George Washington University, Washington, D.C. 20052, United States

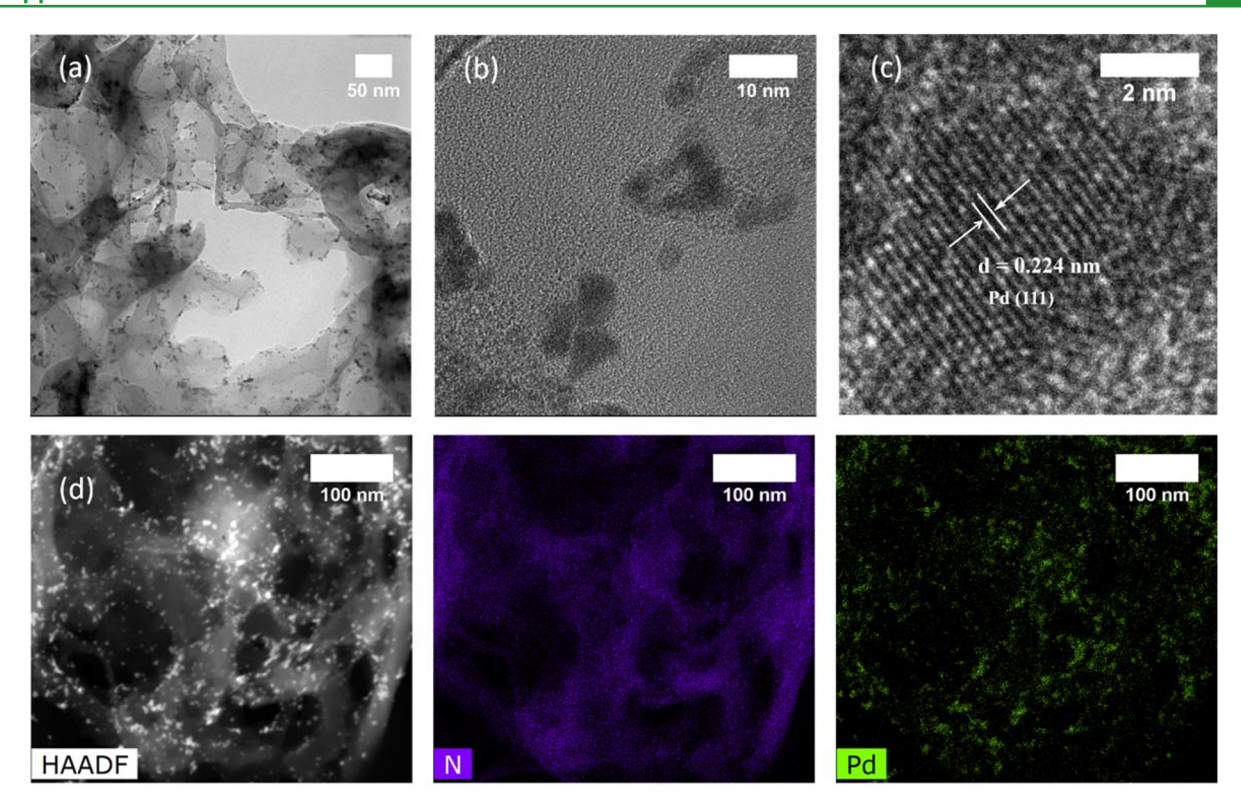


Figure 1. (a, b) Transmission electron microscopy (TEM) of Pd/MCB-EG with (c) a lattice spacing indicated; (d) high-angle annular dark-field–scanning transmission electron microscopy (HAADF-STEM) of Pd/MCB-EG, and the corresponding energy-dispersive X-ray spectroscopy (EDX) elemental mappings for N and Pd.

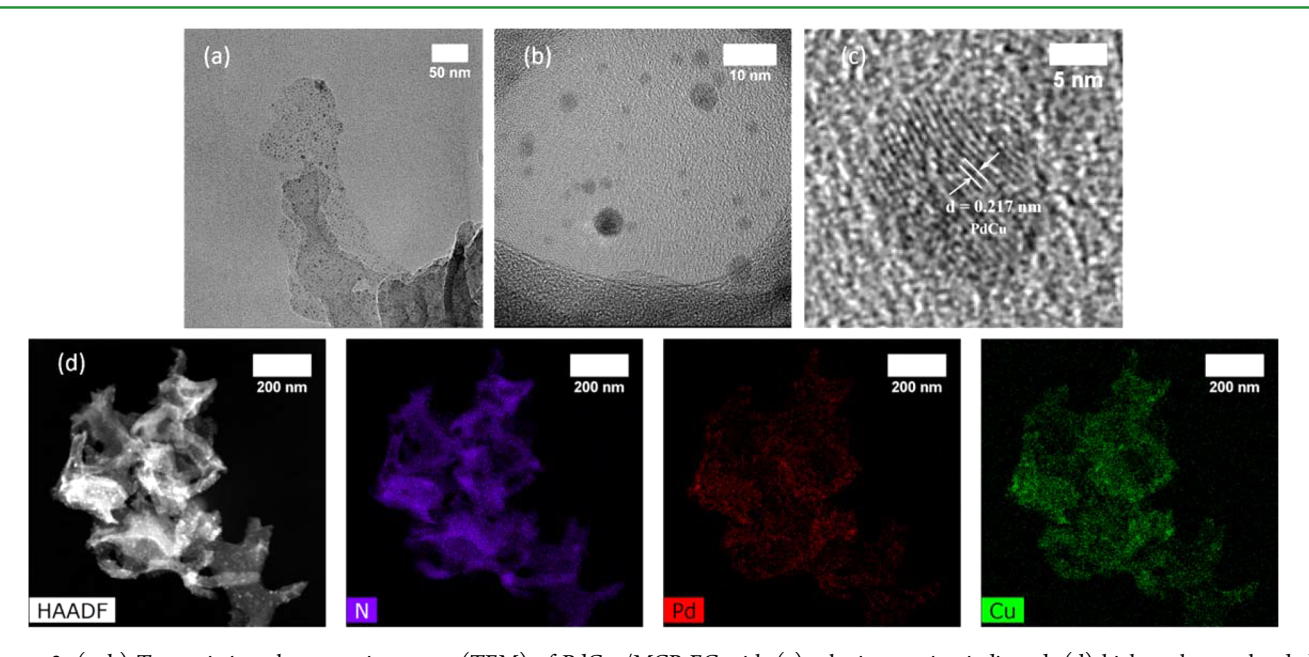


Figure 2. (a, b) Transmission electron microscopy (TEM) of $PdCu_9/MCB-EG$ with (c) a lattice spacing indicated; (d) high-angle annular dark-field—scanning transmission electron microscopy (HAADF-STEM) of $PdCu_9/MCB-EG$, and the corresponding energy dispersive X-ray spectroscopy (EDX) elemental mappings for N, Pd, and Cu.

g- C_3N_4 samples were prepared with different precursors, i.e., melamine, urea, and a supramolecular complex of melamine, cyanuric acid, and barbituric acid via thermal polycondensation (denoted as M, U, and MCB).¹¹ Pd NPs supported on M, U, and MCB were prepared by incipient wetness, and subsequent NaBH₄ reduction or thermal H₂ reduction (i.e., Pd/M-BH, Pd/U-BH, Pd/MCB-BH, and Pd/MCB-H₂).¹² Ethylene glycol

(EG) reduction was used to load Pd and Pd—Cu NPs on MCB, i.e., Pd/MCB-EG and PdCu_x/MCB-EG, and it is advantageous because it was conducted under a mild condition (125 °C), maintained the integrity of g-C₃N₄, and facilitated metal NP dispersion (see results). All theoretical Pd or Cu loadings were 5 or x wt % to the support (x = 4–11). Experimental details are included in the Supporting Information.

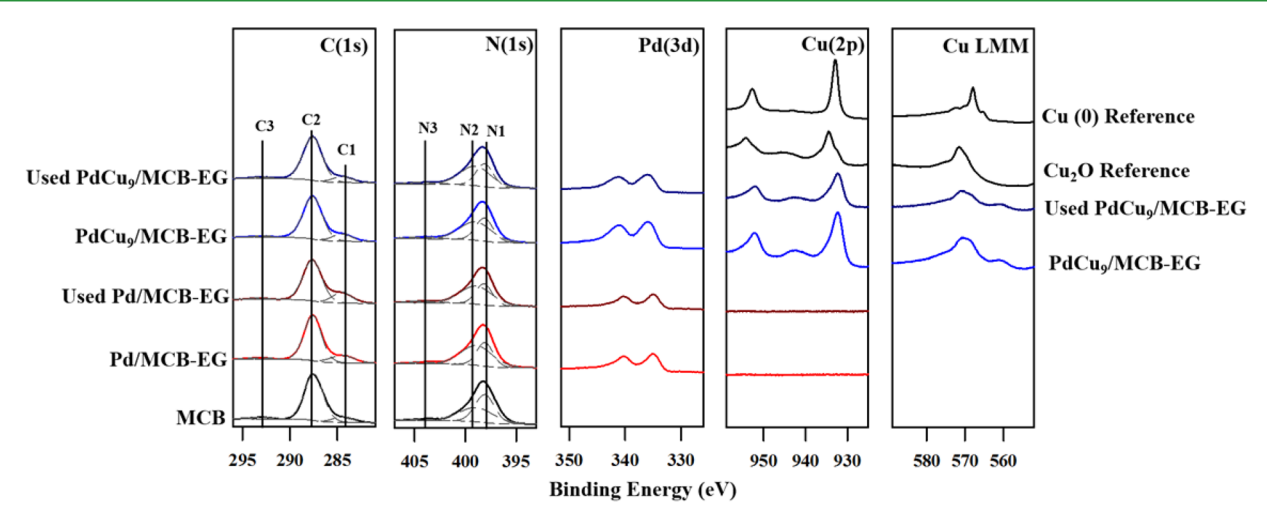


Figure 3. X-ray photoelectron spectroscopy of MCB, fresh and used Pd/MCB-EG, and fresh and used PdCu₉/MCB-EG. Spectra for copper metal and Cu₂O are also included as references for Cu(0) and Cu(I) identification. C1: adventitious carbon (-C-H or -C-C-); C2: sp² carbon (-N=C-); C3: $\pi-\pi^*$; N1: sp² nitrogen (-C-N=C-); N2: terminal N-C(3); and N3: $\pi-\pi^*$.

Pd NP size of Pd/M-BH (4.5 \pm 1.0 nm) was slightly larger than that of Pd/U-BH (3.3 \pm 0.8 nm), Pd/MCB-H₂ (2.9 \pm 0.9 nm), Pd/MCB-BH (3.6 \pm 0.8 nm), and Pd/MCB-EG (2.5 \pm 0.6 nm) (Figure 1 and Figures S1 and S2). Pd NPs aggregated as clusters in Pd/M-BH (Figure S1b), whereas Pd NPs were uniformly distributed in other samples. The high-resolution transmission electron microscopy (HRTEM) (Figure 1b, c) revealed that the Pd NPs were crystalline, and the observed lattice spacing of 0.224 nm is in agreement with that of the Pd(111) crystal plane. 13 For bimetallic PdCu₉/MCB-EG, Pd-Cu NPs were well-dispersed on MCB with an average diameter of 2.3 ± 0.7 nm (Figure 2a, b). The lattice spacing of 0.217 nm, which is in between that of Cu(111) and Pd(111) crystal planes (0.209 and 0.224 nm, respectively), can be indexed to the (111) crystal plane for highly crystalline, face-centered cubic (fcc) Pd-Cu alloys (Figure 2c). 13 The energy-dispersive X-ray spectroscopy (EDX) elemental mappings (Figures 1d and 2d) showed that both Pd and Cu were homogeneously distributed throughout the samples. The porous structure of MCB was maintained after the loading of Pd and Cu by EG reduction, as confirmed by scanning electron microscopy (SEM) (Figure S3).¹¹

X-ray photoelectron spectroscopy (XPS) was used to characterize the bonding environment and oxidation state of the catalysts. Figure 3 shows the C(1s), N(1s), Pd(3d), and Cu(2p) regions for representative catalysts and MCB. Three primary carbon species located at ca. 284.5, 287.5, and 293.1 eV were observed in the C(1s) region (Table S1), in agreement with our previous study. Analysis of the N(1s) region revealed three regions characteristic of g-C₃N₄ (i.e., ca. 398.1, 398.9, and 404.3 eV) (Table S1). No significant changes to the C(1s) and N(1s) regions were apparent for each sample containing Pd or Pd-Cu, indicating that the metals did not chemically bind to the support. 14 Together, XPS, SEM analysis (Figure S3), and X-ray powder diffraction (XRD, Figure S4) demonstrate that g-C₃N₄ kept its physical and chemical structure after Pd and/or Cu loading. 11,14 For Pd/MCB-EG, there was a $Pd(3d_{5/2}/3d_{3/2})$ doublet in the Pd(3d) region consistent with the presence of a single species. The $Pd(3d_{5/2})$ binding energy was located at 335.0 eV (±0.1 eV), indicative of metallic Pd. 15 A slight shoulder on the higher binding energy side of the peaks suggests some oxidized Pd was present, most

likely unreduced Pd2+ adsorbed on the surface. For PdCu₉/ MCB-EG, the $Pd(3d_{5/2})$ peak was broader, centered at a binding energy of 335.9 (±0.2 eV), also suggesting the Pd surface was oxidized. Analysis of the Cu(2p) region for PdCu₉/ MCB-EG revealed two peaks consistent with a $Cu(2p_{3/2}/2p_{1/2})$ doublet, with a Cu $2p_{3/2}$ peak position (932.4 \pm 0.1 eV) that could be from either Cu(0) or Cu(I) species. To distinguish between Cu(0) and Cu(I), inspection of both the Cu(2p) Xray photoelectron transition and the Cu(LMM) Auger line shapes was required. 16,17 Comparison of the Cu(2p) and Cu(LMM) of PdCu₉/MCB-EG to reference spectra obtained in the same instrument showed that the Cu was present as Cu(I). In PdCu₉/MCB-EG, a slight "shake up" peak at ca. 942.0 eV was also observed, indicating that some Cu(II) was also present. Though we did not observe Cu(0) for EG reduced catalysts, which is required for nitrate reduction, Cu(I) could be reduced to Cu(0) with the presence of Pd in nitrate hydrogenation, or Cu(I) may also be a reactive species for nitrate reduction. 18,19

Catalytic performance of Pd supported on g-C₃N₄ for nitrite reduction was evaluated. In our preliminary experiments, light irradiation inhibited catalytic activity for nitrite degradation, likely due to the photoactivity of g-C₃N₄. To avoid the adverse impact of light irradiation on reactivity, we conducted all the experiments in the dark. Pd/MCB-EG showed a catalytic activity similar to Pd/U-BH, Pd/MCB-BH, and Pd/MCB-H₂ for nitrite hydrogenation (Figure 4 and Table S2). The catalytic activity of these samples was 3.0-3.5 fold higher compared to that of Pd/M-BH for nitrite hydrogenation. Initial turnover frequency (TOF₀) for nitrite reduction, i.e., the number of nitrite reduced per Pd site per time at the beginning of the reaction, was similar for Pd/MCB-EG, Pd/U-BH, Pd/MCB-BH, and Pd/MCB-H₂, but was 2.5 fold higher than that of Pd/ M-BH (Table S2). These results are in contrast to our previous observation that TOF₀ of near-spherical Pd NPs was the same for nitrite reduction under the same test condition (e.g., H₂ supply, pH, initial nitrite concentration), regardless of the NP size.8 The discrepancy indicates that factors other than metal dispersion, may also impact catalytic activity. The surface area of U and MCB are significantly larger than that of M (Table S3), and it may result in enhanced mass transfer of reactants and TOF₀ during reaction. 11,20

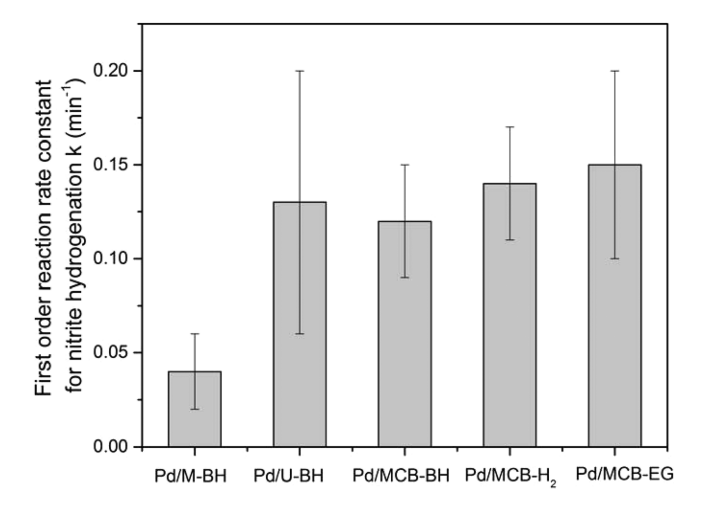


Figure 4. Nitrite reaction rate constants of Pd/M-BH, Pd/U-BH, Pd/MCB-BH, Pd/MCB-H₂, and Pd/MCB-EG. Experimental details are described in the Supporting Information.

Figure 5a exhibits a volcano-shape relationship of nitrate reduction rate constants with increasing Cu loading in PdCu_x/ MCB-EG. The rate constant increased from $(4.1 \pm 0.1) \times 10^{-3}$ to $(3.1 \pm 0.7) \times 10^{-2} \text{ min}^{-1}$ with a Cu loading increasing from 4 to 9 wt %. The time course of nitrate and nitrite concentration for nitrate hydrogenation on PdCu_o/MCB-EG is shown in Figure S5. Further increase in the Cu loading to 11 wt % lowers the reactivity steadily to $(1.7 \pm 0.4) \times 10^{-2} \,\mathrm{min}^{-1}$. Cu is essential for nitrate reduction, and a low Cu loading leads to slow reduction kinetics of nitrate. However, further increase in Cu in the Pd-Cu alloys limits the number of reactive Pd sites for hydrogen dissociation and reductant supply, which also in turn reduces the reactivity. 12,20 Therefore, an optimum Cu loading exists to promote the reactivity for nitrate reduction. The optimal Cu loading was relatively high compared to those found by other studies (Table S4). A previous study suggests that Pd-Cu NPs prepared on lignocellulose via H2 thermal reduction form both alloys and monometallic Pd or Cu NPs. 12 It is likely that EG reduction also results in the formation of both alloys and monometallic NPs, or Pd and Cu NPs that are not in close proximity with each other.²¹ The separation of Pd

and Cu may change the optimum metal composition of catalysts developed by different methods for nitrate reduction.

In addition to the catalytic activity, selectivity toward ammonium, i.e., the molar ratio of produced ammonium to the initial nitrite or nitrate, was also evaluated at the end of hydrogenation (i.e., when nitrite or nitrate concentration decreased below the detection limit). No ammonia was expected in our system because of low pH of CO₂ buffered reaction solution (pH 5.5) and a high pK_a of ammonium (9.24). As shown in Scheme 1, NO plays a critical role in determining the final end-products (i.e., toxic ammonia/ammonium and harmless nitrogen gas).¹⁰ Ammonia/ammonium is a byproduct because of its adverse impacts to human health and ecological systems. Ammonia/ammonium and nitrogen gas are the only end products for nitrite and nitrate hydrogenation when a sufficient reaction time and hydrogen supply is allowed. ¹⁰ Therefore, lower selectivity toward ammonia/ammonium production indicates higher selectivity for nitrogen gas and vice versa, and the catalyst with low ammonia/ammonium selectivity is beneficial for environmental remediation.

In our study, ammonium selectivity of Pd/MCB-EG, Pd/ MCB-BH, and Pd/MCB-H₂ for nitrite reduction was 0.70 \pm 0.06%, $0.96 \pm 0.04\%$, and $0.71 \pm 0.08\%$, respectively; and the ammonium selectivity of PdCu₉/MCB-EG for nitrate reduction was $5.13 \pm 1.58\%$ (Table S5). Ammonium selectivity for nitrate reduction was higher than that for nitrite reduction, likely due to a low concentration of N-containing intermediates and the inhibition of N-N coupling for nitrogen gas production in nitrate reduction. Nitrite, an important reactant that determines ammonium selectivity, showed a much lower concentration for nitrate reduction in contrast to nitrite reduction (µM vs mM, Figure S5). The ammonium selectivity is much lower than that of other supported catalysts, although the same catalyst metals (i.e., Pd and Pd-Cu) and similar experimental conditions (e.g., pH, initial nitrite/nitrate concentration) were used (Table S4). Small NP size is believed to promote ammonia/ammonium production, due to the presence of abundant edges and corners on NPs facilitating N–H interaction. ^{22,23} A high content of Cu may also enhance ammonia/ammonium production, likely due to the segregation of Pd atoms on NPs, suppressing N-N coupling.²³ Our g-C₃N₄ supported Pd and Pd-Cu catalysts have extremely small NP sizes and a high Cu content;

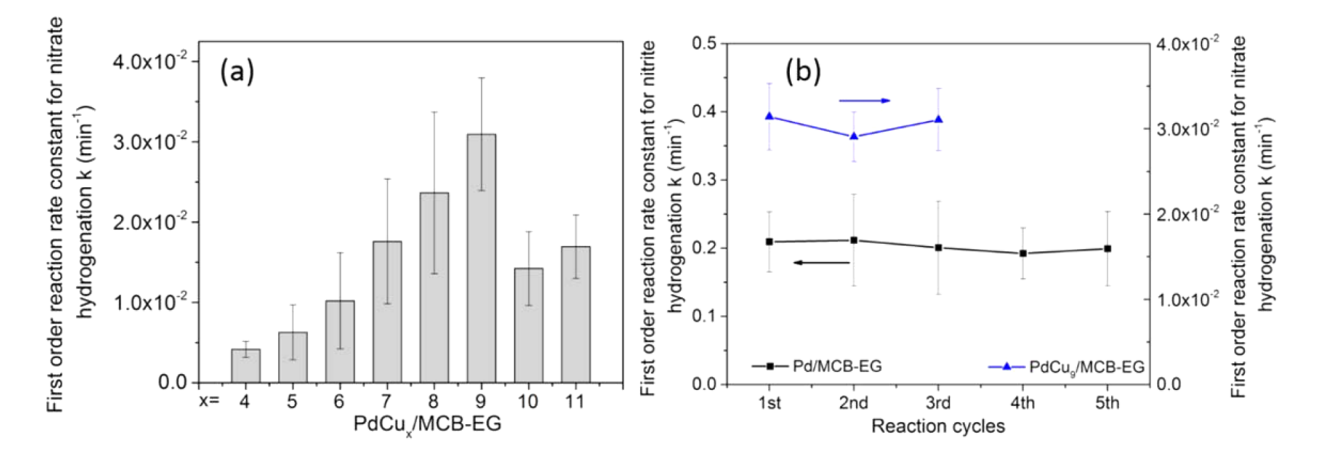


Figure 5. (a) Nitrate reaction rate constants of $PdCu_x/MCB-EG$, and 5 and x wt % of Pd and Cu were loaded to the support (x = 4-11). (b) Nitrite and nitrate reaction rate constants of Pd/MCB-EG and $PdCu_9/MCB-EG$ over multiple cycles of reactions. Experimental details are described in the Supporting Information.

nevertheless, they only produce negligible amount of ammonium. One possible explanation of low ammonium production for our catalysts is that the porous structure of g-C₃N₄ (i.e., MCB) improves mass transfer of reactants. For example, fast diffusion of N-containing reactants and intermediates in nitrite and nitrate reduction promotes N-N coupling and the formation of nitrogen gas over ammonia/ ammonium. Hydroxyl ions are released as a byproduct in nitrate and nitrite hydrogenation, and high pH promotes ammonia/ammonium formation. Fast diffusion and neutralization of hydroxyl ions controls the local pH in catalyst pores and limits ammonia/ammonium production. 22,24 However, Pd supported on nonporous M (prepared by EG) also showed negligible ammonium production for nitrite reduction (below the detection limit of 0.11%, data not shown). Therefore, low ammonium selectivity of g-C₃N₄ supported Pd-based catalysts cannot be attributed to the impact of metal NP size and composition, support porosity, and catalyst preparation methods. Compared with other catalyst supports in Table S4, low ammonium production could be associated with the nature of g-C₃N₄, e.g., abundant N-containing functional groups, which is currently explored by our research group.

Catalyst longevity was tested in 3-5 cycles of nitrite or nitrate reduction, and the results are shown in Figure 5b and Figure S6 and Table S5. Reactivity and ammonium selectivity was retained for nitrite and nitrate reduction on Pd/MCB-EG and PdCu₉/MCB-EG, respectively, when a new batch of nitrite or nitrate solution with recycled catalysts was used for each cycle (Figure 5b). However, all catalysts gradually lost their activity over multiple cycles, when nitrite or nitrate was amended at the beginning of each cycle continuously for the same solution (Figure S6). Specifically, PdCu₉/MCB-EG lost almost 70% of its original activity after 3 cycles of nitrate reduction (Figure S6b). The metal loadings in both fresh and used catalysts (i.e., Pd/MCB-EG and PdCu₉/MCB-EG) were close, and a small amount of Cu was lost after catalyst use indicated by the XPS analysis (Table S6). Inductively coupled plasma-mass spectrometry (ICP-MS) analysis (Table S7) also indicated that the amount of metals leached into the reaction solution was negligible (less than 0.1 wt % of Pd or Cu to the total Pd or Cu loading), and the solid catalyst samples showed limited amount of Cu loss after use. TEM analysis (Figures S7) showed that the NP size of the catalysts increased slightly (by ca. 0.8 to 1.5 nm, Table S8). Moreover, the fresh and used catalysts did not show any noticeable change in the catalyst structure, chemical bonding, and oxidation state (Figures 3 and Figure S4). These results indicated that the loss of the catalytic activity was not mainly from leaching, agglomeration, or oxidation of the metals. The accumulation of bicarbonate (HCO₃⁻), resulting from the reaction between CO₂ and hydroxide produced in nitrite or nitrate hydrogenation, deactivated the Pd and Pd-Cu catalysts because the anion competes with nitrite or nitrate for adsorption on catalytic sites.25

In conclusion, we fabricated g-C₃N₄ supported ultrafine Pd and Pd-Cu NPs for catalytic hydrogenation of waterborne contaminants, nitrite and nitrate, and the optimized catalysts showed high reactivity for contaminant degradation, excellent selectivity for nitrogen gas over ammonium production, and stability over multiple reaction cycles. g-C₃N₄ supports produce very small metal NPs (1–5 nm) for catalytic reactions, by taking advantage of its hydrophilic nature, abundant N-containing groups, and porous structures. EG reduction

effectively loaded Pd and Pd—Cu NPs on the catalyst support, with improved catalytic performance and sustainability for catalyst synthesis. Our study sheds light on the development of innovative monometallic and bimetallic catalysts on an emerging support of g-C₃N₄, and the catalysts can be translated to a broad range of applications, including chemical synthesis, renewable energy production, and environmental remediation.

ASSOCIATED CONTENT

S Supporting Information

The Supporting Information is available free of charge on the ACS Publications website at DOI: 10.1021/acsami.7b09192.

Details of catalyst synthesis and characterization; nitrite and nitrate hydrogenation experiments; mass transfer rate evaluation (PDF)

AUTHOR INFORMATION

Corresponding Author

*E-mail: danmengshuai@gwu.edu, Phone: 202-994-0506.

ORCID ®

Tao Ye: 0000-0003-4768-1811

Danmeng Shuai: 0000-0003-3817-4092

Notes

The authors declare no competing financial interest.

ACKNOWLEDGMENTS

This research was supported by the National Science Foundation (NSF) grant CBET-1437989, startup funds from the Department of Civil and Environmental Engineering, The George Washington University (GW), and the Johns Hopkins University Water SEED grant for supporting our study. We are grateful to the Air Force Office of Scientific Research for funding, and Johns Hopkins University and the U.S. Naval Academy for facilities support.

■ REFERENCES

- (1) Wang, L.; Wang, C.; Hu, X.; Xue, H.; Pang, H. Metal/Graphitic Carbon Nitride Composites: Synthesis, Structures, and Applications. *Chem. Asian J.* **2016**, *11*, 3305–3328.
- (2) Gong, Y.; Li, M.; Li, H.; Wang, Y. Graphitic Carbon Nitride Polymers: Promising Catalysts or Catalyst Supports for Heterogeneous Oxidation and Hydrogenation. *Green Chem.* **2015**, *17*, 715–736.
- (3) Zhang, P.; Jiang, F.; Chen, H. Enhanced Catalytic Hydrogenation of Aqueous Bromate over Pd/Mesoporous Carbon Nitride. *Chem. Eng. J.* **2013**, 234, 195–202.
- (4) Li, X.-H.; Wang, X.; Antonietti, M. Mesoporous $g-C_3N_4$ Nanorods as Multifunctional Supports of Ultrafine Metal Nanoparticles: Hydrogen Generation from Water and Reduction of Nitrophenol with Tandem Catalysis in One Step. *Chem. Sci.* **2012**, 3, 2170–2174.
- (5) Fu, Y.; Huang, T.; Jia, B.; Zhu, J.; Wang, X. Reduction of Nitrophenols to Aminophenols under Concerted Catalysis by Au/g-C₃N₄ Contact System. *Appl. Catal., B* **2017**, 202, 430–437.
- (6) Bruning-Fann, C. S.; Kaneene, J. B. The Effects of Nitrate, Nitrite and *N-N*itroso Compounds on Human Health: A Review. *Vet. Hum. Toxicol.* **1993**, *35*, 521–538.
- (7) Chaplin, B. P.; Reinhard, M.; Schneider, W. F.; Schüth, C.; Shapley, J. R.; Strathmann, T. J.; Werth, C. J. Critical Review of Pd-Based Catalytic Treatment of Priority Contaminants in Water. *Environ. Sci. Technol.* **2012**, *46*, 3655–3670.
- (8) Shuai, D.; Choe, J. K.; Shapley, J. R.; Werth, C. J. Enhanced Activity and Selectivity of Carbon Nanofiber Supported Pd Catalysts for Nitrite Reduction. *Environ. Sci. Technol.* **2012**, *46*, 2847–2855.

- (9) Shuai, D.; McCalman, D. C.; Choe, J. K.; Shapley, J. R.; Schneider, W. F.; Werth, C. J. Structure Sensitivity Study of Waterborne Contaminant Hydrogenation Using Shape- and Size-Controlled Pd Nanoparticles. ACS Catal. 2013, 3, 453–463.
- (10) Zhang, R.; Shuai, D.; Guy, K. A.; Shapley, J. R.; Strathmann, T. J.; Werth, C. J. Elucidation of Nitrate Reduction Mechanisms on a Pd-In Bimetallic Catalyst using Isotope Labeled Nitrogen Species. *ChemCatChem* **2013**, *5*, 313–321.
- (11) Zheng, Q.; Durkin, D. P.; Elenewski, J. E.; Sun, Y.; Banek, N. A.; Hua, L.; Chen, H.; Wagner, M. J.; Zhang, W.; Shuai, D. Visible-Light-Responsive Graphitic Carbon Nitride: Rational Design and Photocatalytic Applications for Water Treatment. *Environ. Sci. Technol.* **2016**, 50, 12938–12948.
- (12) Durkin, D. P.; Ye, T.; Larson, E. G.; Haverhals, L. M.; Livi, K. J. T.; De Long, H. C.; Trulove, P. C.; Fairbrother, D. H.; Shuai, D. Lignocellulose Fiber- and Welded Fiber- Supports for Palladium-Based Catalytic Hydrogenation: A Natural Fiber Welding Application for Water Treatment. ACS Sustainable Chem. Eng. 2016, 4, 5511–5522.
- (13) Li, M.; Wang, J.; Li, P.; Chang, K.; Li, C.; Wang, T.; Jiang, B.; Zhang, H.; Liu, H.; Yamauchi, Y.; Umezawa, N.; Ye, J. Mesoporous Palladium-Copper Bimetallic Electrodes for Selective Electrocatalytic Reduction of Aqueous CO₂ to CO. *J. Mater. Chem. A* **2016**, *4*, 4776–4782.
- (14) Zhang, G.; Zang, S.; Lin, L.; Lan, Z.-A.; Li, G.; Wang, X. Ultrafine Cobalt Catalysts on Covalent Carbon Nitride Frameworks for Oxygenic Photosynthesis. *ACS Appl. Mater. Interfaces* **2016**, 8, 2287–2296.
- (15) Moulder, J. F.; Stickle, W. F.; Sobol, P. E.; Bomben, K. D. *Handbook for X-ray Photoelectron Spectroscopy*; Physical Electronics Inc.: Chanhassen, MN, 1995.
- (16) Batista, J.; Pintar, A.; Mandrino, D.; Jenko, M.; Martin, V. XPS and TPR Examinations of g-Alumina Supported Pd-Cu Catalysts. *Appl. Catal.*, A 2001, 206, 113–124.
- (17) Speckmann, H. D.; Haupt, S.; Strehblow, H. A Quantitative Surface Analytical Study of Electrochemically-Formed Copper Oxides by XPS and X-Ray-Induced Auger Spectroscopy. *Surf. Interface Anal.* 1988, 11, 148–155.
- (18) Gao, W.; Guan, N.; Chen, J.; Guan, X.; Jin, R.; Zeng, H.; Liu, Z.; Zhang, F. Titania Supported Pd-Cu Bimetallic Catalyst for the Reduction of Nitrate in Drinking Water. *Appl. Catal., B* **2003**, *46*, 341–351.
- (19) Barrabés, N.; Sá, J. Catalytic Nitrate Removal from Water, Past, Present and Future Perspectives. *Appl. Catal., B* **2011**, *104*, 1–5.
- (20) Jung, J.; Bae, S.; Lee, W. Nitrate Reduction by Maghemite Supported Cu-Pd Bimetallic Catalyst. *Appl. Catal., B* **2012**, *127*, 148–158.
- (21) Nair, A. A. S.; Sundara, R. Palladium Cobalt Alloy Catalyst Nanoparticles Facilitated Enhanced Hydrogen Storage Performance of Graphitic Carbon Nitride. *J. Phys. Chem. C* **2016**, *120*, 9612–9618.
- (22) Sun, W.; Yang, W.; Xu, Z.; Li, Q.; Shang, J. K. Synthesis of Superparamagnetic Core—Shell Structure Supported Pd Nanocatalysts for Catalytic Nitrite Reduction with Enhanced Activity, No Detection of Undesirable Product of Ammonium, and Easy Magnetic Separation Capability. ACS Appl. Mater. Interfaces 2016, 8, 2035—2047.
- (23) Yoshinaga, Y.; Akita, T.; Mikami, I.; Okuhara, T. Hydrogenation of Nitrate in Water to Nitrogen over Pd—Cu Supported on Active Carbon. *J. Catal.* **2002**, 207, 37—45.
- (24) Chinthaginjala, J. K.; Lefferts, L. Support Effect on Selectivity of Nitrite Reduction in Water. *Appl. Catal., B* **2010**, *101*, 144–149.
- (25) Chaplin, B. P.; Roundy, E.; Guy, K. A.; Shapley, J. R.; Werth, C. J. Effects of Natural Water Ions and Humic Acid on Catalytic Nitrate Reduction Kinetics Using an Alumina Supported Pd—Cu Catalyst. *Environ. Sci. Technol.* **2006**, *40*, 3075–3081.